

Beyond Diagonal Reconfigurable Intelligent Surfaces Utilizing Graph Theory: Modeling, Architecture Design, and Optimization

Matteo Nerini, *Graduate Student Member, IEEE*, Shanpu Shen, *Senior Member, IEEE*,
Hongyu Li, *Graduate Student Member, IEEE*, Bruno Clerckx, *Fellow, IEEE*

Abstract—Recently, beyond diagonal reconfigurable intelligent surface (BD-RIS) has been proposed to generalize conventional RIS. BD-RIS has a scattering matrix that is not restricted to being diagonal and thus brings a performance improvement over conventional RIS. While different BD-RIS architectures have been proposed, it still remains an open problem to develop a systematic approach to design BD-RIS architectures achieving the optimal trade-off between performance and circuit complexity. In this work, we propose novel modeling, architecture design, and optimization for BD-RIS based on graph theory. This graph theoretical modeling allows us to develop two new efficient BD-RIS architectures, denoted as tree-connected and forest-connected RIS. Tree-connected RIS, whose corresponding graph is a tree, is proven to be the least complex BD-RIS architecture able to achieve the performance upper bound in multiple-input single-output (MISO) systems. Besides, forest-connected RIS allows us to strike a balance between performance and complexity, further decreasing the complexity over tree-connected RIS. To optimize tree-connected RIS, we derive a closed-form global optimal solution, while forest-connected RIS is optimized through a low-complexity iterative algorithm. Numerical results confirm that tree-connected (resp. forest-connected) RIS achieves the same performance as fully-connected (resp. group-connected) RIS, while reducing the complexity by up to 16.4 times.

Index Terms—Beyond diagonal reconfigurable intelligent surface (BD-RIS), forest-connected, graph theoretical modeling, tree-connected.

I. INTRODUCTION

Reconfigurable intelligent surface (RIS) is expected to be a key technology in 6G to enhance the performance of wireless systems in an efficient and cost-effective manner [1], [2], [3]. An RIS consists of a large number of reconfigurable scattering elements, each with the capability to manipulate the phase of an incident electromagnetic wave, so that the phase shifts of these elements can be coordinated to direct the scattered electromagnetic signal toward the intended receiver. Owing to the benefits of low power consumption and cost-effective architecture, RIS has gained widespread attention.

In a conventional RIS architecture, each element is independently controlled by a tunable impedance connected to ground [4]. Such architecture, referred to as the single-connected

RIS, results in a diagonal scattering matrix, which is also commonly known as the phase shift matrix. Conventional RIS with diagonal scattering matrix has been widely used to enhance different wireless systems, such as single-cell [5], [6], [7] and multi-cell communications [8], orthogonal frequency division multiplexing (OFDM) [9], non-orthogonal multiple access (NOMA) [10], rate splitting multiple access (RSMA) [11], radio frequency (RF) sensing systems [12], wireless power transfer (WPT) systems [13], and simultaneous wireless information and power transfer (SWIPT) systems [14]. In addition, research has been conducted to optimize RIS based on imperfect channel state information (CSI) [15], [16], in multi-RIS scenarios [17], [18], and with discrete phase shifts to account for practical hardware impairments [19], [20]. Channel estimation protocols with reduced pilot overhead for RIS-aided systems have been proposed [21]. Active RIS have been proposed to overcome the multiplicative fading effect limiting the gains of passive RIS by amplifying the reflected signals via amplifiers integrated into their elements [22], [23]. Furthermore, RIS prototypes have been realized in [24], [25].

Recently, the conventional RIS architecture considered in [5]–[25] has been generalized with the introduction of beyond diagonal RIS (BD-RIS). BD-RIS has a scattering matrix that is not restricted to being diagonal [26], with various architectures and modes available as depicted in the classification tree in Fig. 1. Specifically, group-connected and fully-connected architectures, whereby some or all RIS elements are connected with each other through tunable impedance components, are proposed in [4], generalizing the single-connected architecture to enhance the RIS performance. Subsequently, group- and fully-connected RIS with discrete values are efficiently optimized in [27], while the closed-form global optimal solutions for group- and fully-connected RIS with continuous values are derived in [28]. In addition, the simultaneously transmitting and reflecting RIS (STAR-RIS) or intelligent omni-surface (IOS) is presented in [29], [30], which differs from conventional RIS as signals impinging on this RIS can be both reflected and transmitted through the RIS for a full space coverage. STAR-RIS is generalized in [31] which unifies different BD-RIS modes (reflective/transmissive/hybrid) and different BD-RIS architectures (single-/group-/fully-connected). To further enhance RIS performance while maintaining a full-space coverage, multi-sector BD-RIS is proposed in [32], where the elements are split into multiple sectors with each covering a sector of space. Further, the synergy of multi-sector BD-RIS

Corresponding author: Shanpu Shen.

M. Nerini, H. Li, and B. Clerckx are with the Department of Electrical and Electronic Engineering, Imperial College London, London SW7 2AZ, U.K. (e-mail: {m.nerini20, c.li21, b.clerckx}@imperial.ac.uk).

S. Shen is with the Department of Electrical Engineering and Electronics, University of Liverpool, Liverpool L69 3GJ, U.K. (e-mail: Shanpu.Shen@liverpool.ac.uk).

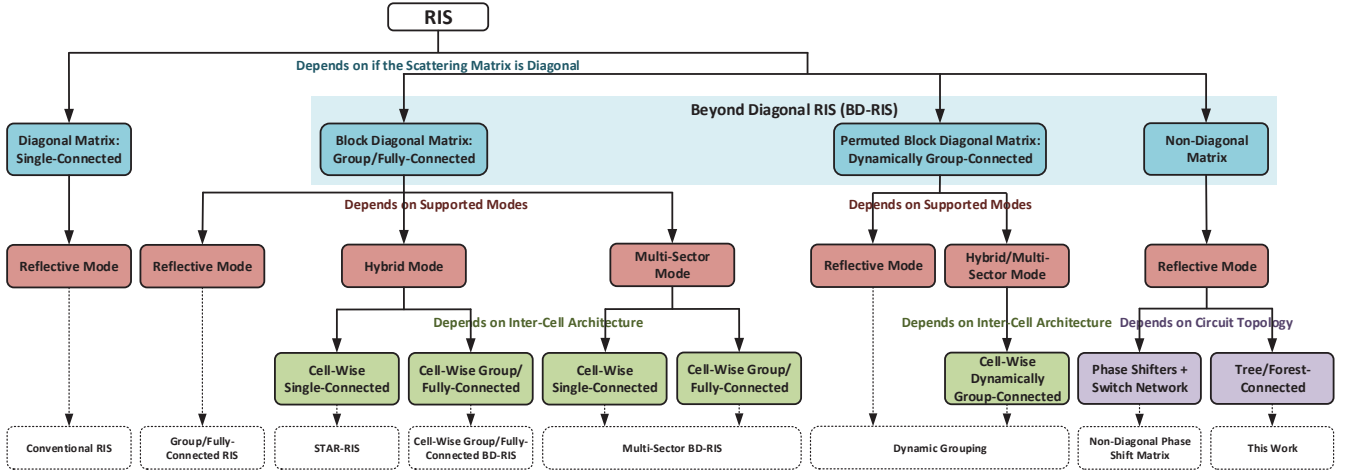


Fig. 1. RIS classification tree.

and RSMA is proved to enlarge the coverage, improve the performance, and save on antennas in multi-user systems [33]. Departing from existing works on BD-RIS with fixed architectures [4], [26]-[33], dynamically group-connected RIS has been proposed in [34], outperforming fixed group-connected RIS by dynamically dividing the RIS elements into groups depending on the channel realization. Besides, a BD-RIS with a non-diagonal phase shift matrix has been proposed in [35], which is able to achieve a higher rate than conventional RIS.

Among all the BD-RISs [4], [26]-[35], the fully-connected architecture provides the highest flexibility and best performance, which is however at the expense of high circuit complexity since it has a large number of tunable impedance components. Although the group-connected architecture can simplify the circuit complexity, it still remains an open problem to develop a systematic approach to design BD-RIS architecture achieving the optimal trade-off between performance and circuit complexity, that is achieving the best performance with the least complexity. To address this issue, in this work, we propose novel modeling, architecture design, and optimization for BD-RIS by utilizing graph theory. The contributions of this paper are summarized as follows.

First, we propose a novel modeling of BD-RIS architectures utilizing graph theory. To the authors' best knowledge, it is the first time that BD-RIS (or any other RIS) architectures are modeled through graph theory. Specifically, we model each BD-RIS architecture by a graph, whose vertices characterize the RIS ports and whose edges characterize the tunable impedance components connecting the RIS ports. This graph theoretical modeling lays down the foundations for developing new efficient BD-RIS architectures.

Second, we derive a necessary and sufficient condition for a BD-RIS architecture to achieve the performance upper bound in multiple-input single-output (MISO) systems. Consequently, we characterize the least complex BD-RISs achieving such an upper bound. The resulting least-complexity BD-RIS architectures are referred to as tree-connected RIS since their corresponding graph is a tree. In addition, two specific examples of tree-connected RIS are proposed, namely tridiagonal RIS

and arrowhead RIS. Tree-connected RIS achieves the same performance in MISO systems as fully-connected RIS with a circuit complexity significantly reduced by 16.4 times, when 64 RIS elements are considered.

Third, we prove that there always exists one and only one global optimal solution to optimize tree-connected RIS. To find this solution, we derive a closed-form algorithm valid for any tree-connected architecture. With this algorithm, tree-connected RIS achieves a performance improvement of 51.7% over single-connected RIS. We show that the proposed algorithm is optimal in single-user as well as multi-user systems.

Fourth, we propose forest-connected RIS as an additional BD-RIS family to reach a trade-off between performance and circuit complexity. Forest-connected RIS serves as a bridge between single- and tree-connected RIS. We propose a low-complexity iterative algorithm to optimize forest-connected RIS. Numerical results show that forest-connected RIS achieves the same performance as group-connected RIS, while reducing the circuit complexity by 2.4 times.

Organization: In Section II, we introduce the graph theoretical modeling of BD-RIS. In Section III, we derive tree- and forest-connected RIS architectures and provide two examples of tree-connected RIS. In Section IV we provide a global optimal closed-form solution to optimize tree-connected RIS and an iterative approach to optimize forest-connected RIS. In Section V, we evaluate the performance of the proposed BD-RISs. Finally, Section VI concludes this work. For reproducible research, the simulation code is available at <https://github.com/matteonerini/bdris-utilizing-graph-theory>.

Notation: Vectors and matrices are denoted with bold lower and bold upper letters, respectively. Scalars are represented with letters not in bold font. $\Re\{a\}$, $\Im\{a\}$, $|a|$, $\arg(a)$, and a^* refer to the real part, imaginary part, modulus, phase, and the complex conjugate of a complex scalar a , respectively. $[\mathbf{a}]_i$ and $\|\mathbf{a}\|$ refer to the i th element and l_2 -norm of a vector \mathbf{a} , respectively. \mathbf{A}^T , \mathbf{A}^H , $[\mathbf{A}]_{i,j}$, and $\|\mathbf{A}\|$ refer to the transpose, conjugate transpose, (i, j) th element, and l_2 -norm of a matrix \mathbf{A} , respectively. $\mathbf{A} \sim \mathbf{B}$ means that the matrices \mathbf{A} and \mathbf{B} are equivalent. \mathbb{R} and \mathbb{C} denote real and complex number

set, respectively. $j = \sqrt{-1}$ denotes imaginary unit. $\mathbf{0}$ and \mathbf{I} denote an all-zero matrix and an identity matrix, respectively. $\mathcal{CN}(\mathbf{0}, \mathbf{I})$ denotes the distribution of a circularly symmetric complex Gaussian random vector with mean vector $\mathbf{0}$ and covariance matrix \mathbf{I} and \sim stands for ‘‘distributed as’’. $\text{diag}(\mathbf{a})$ refers to a diagonal matrix with diagonal elements being the vector \mathbf{a} . $\text{diag}(\mathbf{A}_1, \dots, \mathbf{A}_N)$ refers to a block diagonal matrix with blocks being $\mathbf{A}_1, \dots, \mathbf{A}_N$.

II. BD-RIS MODELING UTILIZING GRAPH THEORY

Consider a MISO system with an M -antenna transmitter and a single-antenna receiver, which is aided by an N -element RIS. The N -element RIS can be modeled as N antennas connected to an N -port reconfigurable impedance network that is characterized by the scattering matrix $\Theta \in \mathbb{C}^{N \times N}$ [4]. We assume the direct channel between the transmitter and receiver is blocked and thus is negligible compared to the indirect channel provided by RIS. Therefore, the overall channel $\mathbf{h} \in \mathbb{C}^{1 \times M}$ between the transmitter and receiver can be written as

$$\mathbf{h} = \mathbf{h}_{RI} \Theta \mathbf{H}_{IT}, \quad (1)$$

where $\mathbf{h}_{RI} \in \mathbb{C}^{1 \times N}$ and $\mathbf{H}_{IT} \in \mathbb{C}^{N \times M}$ are the channel matrices from the RIS to the receiver, and from the transmitter to the RIS, respectively. We denote the transmit signal as $\mathbf{x} = \mathbf{w}s$, where $\mathbf{w} \in \mathbb{C}^{M \times 1}$ is the precoder satisfying $\|\mathbf{w}\| = 1$ and $s \in \mathbb{C}$ is the transmit symbol with power $P_T = E[|s|^2]$. Hence, the received signal is given by $y = \mathbf{h}\mathbf{x} + n$, where n is the additive white Gaussian noise (AWGN).

The N -port reconfigurable impedance network consists of tunable passive impedance components. In addition to S-parameters (the scattering matrix), the N -port reconfigurable impedance network can be also characterized by Y-parameters [36], that is the admittance matrix denoted as $\mathbf{Y} \in \mathbb{C}^{N \times N}$. According to microwave network theory [36], the scattering matrix Θ and admittance matrix \mathbf{Y} are related by

$$\Theta = (\mathbf{I} + Z_0 \mathbf{Y})^{-1} (\mathbf{I} - Z_0 \mathbf{Y}), \quad (2)$$

where Z_0 denotes the reference impedance used for computing the scattering parameter, and usually set as $Z_0 = 50 \Omega$. Furthermore, we have $\mathbf{Y} = \mathbf{Y}^T$ and $\Theta = \Theta^T$ because of the reciprocity of the reconfigurable impedance network. To maximize the power scattered by the RIS, \mathbf{Y} should be purely susceptive and thus writes as $\mathbf{Y} = j\mathbf{B}$, where $\mathbf{B} \in \mathbb{R}^{N \times N}$ denotes the susceptance matrix of the N -port reconfigurable impedance network¹. Hence, Θ is given by

$$\Theta = (\mathbf{I} + jZ_0 \mathbf{B})^{-1} (\mathbf{I} - jZ_0 \mathbf{B}), \quad (3)$$

yielding that Θ is symmetric unitary in the case of reciprocal and lossless RIS. Depending on the circuit topology of the N -port reconfigurable impedance network, the scattering matrix Θ and admittance matrix \mathbf{Y} satisfy different constraints, which results in diagonal RIS and beyond diagonal RIS as follows.

¹In this study, we focus on passive RIS, assumed to be lossless to maximize the reflection gain. However, active RIS with negative resistive components can be considered to further improve the gain [22], [23].

A. Diagonal RIS

In diagonal RIS, each RIS port is not connected to the other ports and is connected to ground through a tunable admittance [4]. Accordingly, the admittance matrix \mathbf{Y} and the scattering matrix Θ are diagonal, written as

$$\mathbf{Y} = \text{diag}(Y_1, Y_2, \dots, Y_N), \quad (4)$$

$$\Theta = \text{diag}(e^{j\theta_1}, e^{j\theta_2}, \dots, e^{j\theta_N}), \quad (5)$$

where Y_n and θ_n are respectively the tunable admittance and phase shift for the n th RIS port for $n = 1, \dots, N$. Such circuit topology is also referred to as single-connected RIS [4] and has been widely adopted [5]-[25].

B. Beyond Diagonal RIS

In BD-RIS, the RIS ports can also be connected to each other through additional tunable admittance components. We denote the tunable admittance connecting the n th port to the m th port as $Y_{n,m}$. According to [37], given the admittance components Y_n and $Y_{n,m}$, the (n, m) th entry of the admittance matrix \mathbf{Y} is given by

$$[\mathbf{Y}]_{n,m} = \begin{cases} -Y_{n,m} & n \neq m \\ Y_n + \sum_{k \neq n} Y_{n,k} & n = m \end{cases}. \quad (6)$$

Thus, by selecting $Y_{n,m} = -[\mathbf{Y}]_{n,m}$ and $Y_n = \sum_k [\mathbf{Y}]_{n,k}$, we can implement an arbitrary symmetric \mathbf{Y} so that the admittance matrix \mathbf{Y} and the scattering matrix Θ are beyond diagonal. Particularly, there are two special categories of BD-RIS, namely fully-connected and group-connected RIS [4]. Due to the enhanced flexibility in \mathbf{Y} and Θ , BD-RIS is proven to outperform single-connected RIS [4], [26]-[35].

C. Graph Theoretical Modeling

To model the general circuit topology of BD-RIS, we resort for the first time to graph theoretical tools [38]. Specifically, we represent the circuit topology of BD-RIS through a graph

$$\mathcal{G} = (\mathcal{V}, \mathcal{E}), \quad (7)$$

where \mathcal{V} represents the *vertex set* of \mathcal{G} and is given by the set of indices of RIS ports, i.e.

$$\mathcal{V} = \{1, 2, \dots, N\}, \quad (8)$$

and \mathcal{E} represents the *edge set* of \mathcal{G} and is given by

$$\mathcal{E} = \{(n_\ell, m_\ell) \mid n_\ell, m_\ell \in \mathcal{V}, Y_{n_\ell, m_\ell} \neq 0, n_\ell \neq m_\ell\}. \quad (9)$$

Thus, there exists an edge between vertex n_ℓ and vertex m_ℓ if and only if there is a tunable admittance connecting port n_ℓ and port m_ℓ , namely the ℓ th admittance. Accordingly, given a graph \mathcal{G} with edge set $\mathcal{E} = \{(n_\ell, m_\ell)\}_{\ell=1}^L$, the corresponding BD-RIS admittance matrix has $2L$ non-zero off-diagonal entries, i.e. $[\mathbf{Y}]_{n_\ell, m_\ell}$ and $[\mathbf{Y}]_{m_\ell, n_\ell}$ for $\ell = 1, \dots, L$, while the other off-diagonal entries are zero. In the following, we define the circuit complexity of a BD-RIS architecture as the number of tunable admittance components in its circuit topology. Thus, the circuit complexity of a BD-RIS represented by a graph with L edges is given by $N + L$ since it includes N tunable

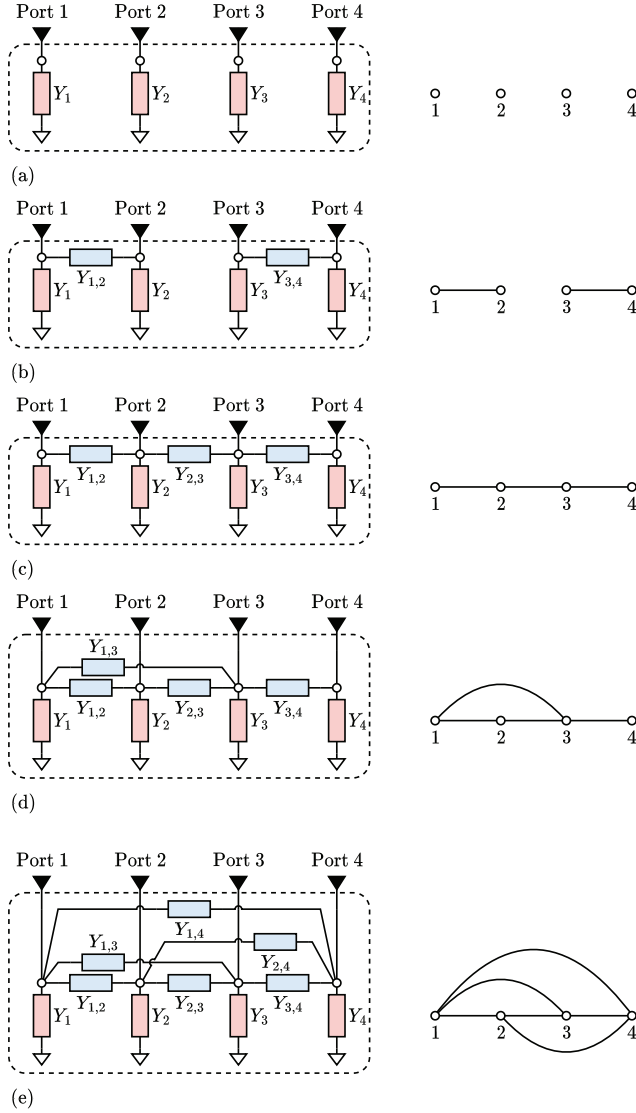


Fig. 2. Examples of 4-port BD-RIS architectures (left) and their corresponding graphs \mathcal{G} (right), where \mathcal{G} is (a) empty, (b) disconnected and acyclic, (c) connected and acyclic, i.e., a tree, (d) connected and cyclic, (e) complete.

admittance components connecting each element to ground, and L tunable admittance components interconnecting the elements to each other.

To better clarify our graph theoretical modeling of BD-RIS, we show a 4-element single-connected RIS with its associated graph in Fig. 2(a), and four examples of 4-element BD-RIS with their associated graphs in Fig. 2(b)-(e). We also use Fig. 2 to illustrate the graph theoretical definitions [38] that are used in this work, as briefly summarized in the following.

- A graph is *empty* when there is no edge.
- A graph is *connected* when there is a *path*, i.e., a finite sequence of distinct edges joining a sequence of distinct vertices, from any vertex to any other vertex.
- A graph that is not connected is called *disconnected*.
- A *cyclic* graph is a graph containing at least one *cycle*, i.e., a finite sequence of distinct edges joining a sequence of vertices, where only the first and last vertices are equal.

- A graph that is not cyclic is called *acyclic*, or a *forest*.
- A *tree* is defined as a connected and acyclic graph.
- A graph is *complete* when each pair of distinct vertices is joined by an edge.
- A graph is *simple* when there is no edge with identical ends (called *loops*) and no multiple edges joining the same pair of vertices.

Given these definitions, we recognize that the graph for the single-connected RIS in Fig. 2(a) is empty, the graph in Fig. 2(b) is disconnected and acyclic, the graph in Fig. 2(c) is connected and acyclic, i.e., a tree, the graph in Fig. 2(d) is connected and cyclic as it presents the cycle $1 - 2 - 3$, and the graph for the fully-connected RIS in Fig. 2(e) is complete. In addition, graphs associated with BD-RIS are always simple². Therefore, graph theory is effective to characterize and model the circuit topology of BD-RIS and the corresponding admittance matrix \mathbf{Y} .

Utilizing graph theory, we propose two novel families of BD-RIS with remarkable properties, which are referred to as tree-connected RIS and forest-connected RIS, in the following section.

III. BD-RIS ARCHITECTURE DESIGN UTILIZING GRAPH THEORY

A. Tree-Connected RIS

As a starting point, we investigate how the graph of BD-RIS influences the system performance. To that end, we formulate the BD-RIS optimization problem for MISO systems utilizing graph theory. Specifically, we assume the BD-RIS is lossless and purely susceptive and aim to maximize the received signal power $P_R = P_T |\mathbf{h}_{RI} \Theta \mathbf{H}_{IT} \mathbf{w}|^2$ by jointly optimizing \mathbf{w} and Θ ³. Thus, we can formulate the problem as

$$\max_{\Theta, \mathbf{w}} P_T |\mathbf{h}_{RI} \Theta \mathbf{H}_{IT} \mathbf{w}|^2 \quad (10)$$

$$\text{s.t. } \Theta = (\mathbf{I} + jZ_0 \mathbf{B})^{-1} (\mathbf{I} - jZ_0 \mathbf{B}), \quad (11)$$

$$\mathbf{B} = \mathbf{B}^T, \quad (12)$$

$$\mathbf{B} \in \mathcal{B}_{\mathcal{G}}, \quad (13)$$

$$\|\mathbf{w}\| = 1, \quad (14)$$

where $\mathcal{B}_{\mathcal{G}}$ represents the set of possible susceptance matrices of BD-RISs characterized by the graph $\mathcal{G} = (\mathcal{V}, \mathcal{E})$ and is written as

$$\mathcal{B}_{\mathcal{G}} = \{\mathbf{B} | [\mathbf{B}]_{n,m} = 0, n \neq m, n, m \in \mathcal{V}, (n, m) \notin \mathcal{E}\} \quad (15)$$

which means that an off-diagonal entry is zero if there exists no corresponding edge in the graph. The graph \mathcal{G} is fixed in (10)-(14) since the interconnections between the RIS elements are fixed to avoid additional circuit complexity. Note that problem (10)-(14) considers the optimization of the RIS based

²In this work, we consider graphs where the edges are not oriented since we assume the RIS to have a reciprocal reconfigurable impedance network. BD-RIS architectures with non-reciprocal reconfigurable impedance networks could be modeled through *directed* graphs, i.e., graphs with oriented edges, but are beyond the scope of this work.

³Maximizing the received signal power or the achievable rate are equivalent problems in single-user systems. Thus, we consider the received signal power since it is independent of the noise power.

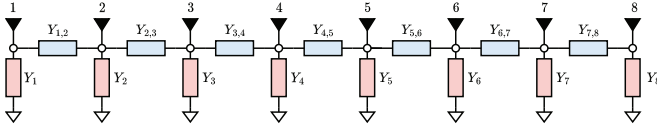


Fig. 3. Tridiagonal RIS with $N = 8$.

on the instantaneous channel, as typically performed in related literature [1], [2], [3]. Perfect CSI is assumed, which can be obtained with the semi-passive channel estimation protocol discussed in [3].

From (10)-(14), we can deduce that the maximum received signal power depends on the graph of the BD-RIS. Specifically, when the graph \mathcal{G} has more edges, the susceptance matrix \mathbf{B} is more flexible so that the maximum received signal power is higher. However, the enhanced performance is achieved at the expense of higher circuit complexity (more connections from the increased number of edges). Thus, it is worth designing the graph of BD-RIS to achieve the best performance with the least complexity.

To that end, we first consider the case that the graph \mathcal{G} is complete, that is the fully-connected RIS. As shown in [4] and [28], maximum ratio transmission (MRT) gives the optimal \mathbf{w} and subsequently the fully-connected RIS can achieve the upper bound of the received signal power given by

$$\bar{P}_R = P_T \|\mathbf{h}_{RI}\|^2 \|\mathbf{H}_{IT}\|^2, \quad (16)$$

following the sub-multiplicativity of the l_2 -norm and that $\Theta^H \Theta = \mathbf{I}$. Leveraging this upper bound, herein we define a BD-RIS that achieves the performance upper bound \bar{P}_R for any channel realization as MISO optimal. Thus, the fully-connected RIS is MISO optimal. More generally, the following lemma provides a sufficient and necessary condition for a BD-RIS to be MISO optimal.

Lemma 1. *A BD-RIS with associated graph \mathcal{G} is MISO optimal if and only if \mathcal{G} is a connected graph.*

Proof. Please refer to Appendix A. \square

Using Lemma 1, we have the following proposition providing the least complexity for MISO optimal BD-RIS.

Proposition 1. *The minimum number of edges in the graph of a MISO optimal BD-RIS is $N - 1$, with N denoting the number of RIS elements.*

Proof. Please refer to Appendix B. \square

Remarkably, a connected graph \mathcal{G} on N vertices with $N - 1$ edges is a tree. To show this, we observe that removing any edge from \mathcal{G} makes the graph disconnected because of Proposition 1. Thus, \mathcal{G} cannot have a cycle and must be a tree (connected and acyclic). Therefore, to minimize the BD-RIS circuit complexity while maintaining optimal performance, we propose tree-connected RIS as BD-RIS whose corresponding graph is a tree. According to this definition, tree-connected RIS includes N admittance components connecting each port to ground and $N - 1$ admittance components interconnecting the ports to each other, yielding a total of $2N - 1$ admittance

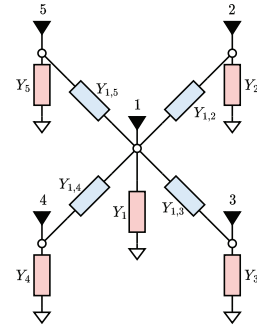


Fig. 4. Arrowhead RIS with $N = 5$ where port 1 is the central vertex.

components, which is much less than the $N(N + 1)/2$ admittance components in fully-connected RIS.

B. Two Examples of Tree-Connected RIS

Tree-connected RIS refers to a family of BD-RISs, including multiple possible architectures. To clarify the concept of tree-connected RIS, in this subsection we provide two specific examples of tree-connected RIS, referred to as tridiagonal and arrowhead RIS.

1) *Tridiagonal RIS:* We define tridiagonal RIS as tree-connected RIS whose graph \mathcal{G} is a *path graph*. In graph theory, the degree of a vertex is defined as the number of edges incident with it, and a path graph is defined as a graph where two vertices have *degree* one and all the others (if any) have degree two [38]. The vertex set of the graph associated with tridiagonal RIS is defined as

$$\mathcal{V}^{\text{Tri}} = \{n_1, n_2, \dots, n_N\}, \quad (17)$$

and the edge set can be expressed accordingly as

$$\mathcal{E}^{\text{Tri}} = \{(n_\ell, n_{\ell+1}) \mid \ell = 1, \dots, N - 1\}. \quad (18)$$

Interestingly, the tridiagonal architectures have also been proposed to realize low-complexity impedance matching networks for multiple antenna systems [37]. In Fig. 3, we provide an illustrative example of tridiagonal RIS with $N = 8$. As a consequence of such architecture, the susceptance matrix of tridiagonal RIS is symmetric and tridiagonal ($[\mathbf{B}]_{i,j} = 0$ if $|i - j| > 1$), written as

$$\mathbf{B} = \begin{bmatrix} [\mathbf{B}]_{1,1} & [\mathbf{B}]_{1,2} & \cdots & 0 \\ [\mathbf{B}]_{1,2} & [\mathbf{B}]_{2,2} & \ddots & \vdots \\ \vdots & \ddots & \ddots & [\mathbf{B}]_{N-1,N} \\ 0 & \cdots & [\mathbf{B}]_{N-1,N} & [\mathbf{B}]_{N,N} \end{bmatrix}. \quad (19)$$

Note that if the port indexes in \mathcal{V}^{Tri} are permuted, \mathbf{B} is a permuted tridiagonal matrix.

2) *Arrowhead RIS:* We define arrowhead RIS as tree-connected RIS whose graph \mathcal{G} is a *star graph*. In graph theory, a star graph is defined as a graph where at most one vertex, called *central*, has degree greater than one and all the others have degree one [38]. Accordingly, the vertex set of the graph associated with arrowhead RIS is defined as

$$\mathcal{V}^{\text{Arrow}} = \{c, n_1, n_2, \dots, n_{N-1}\}, \quad (20)$$

where c denotes the central vertex, while the edge set is consequently expressed as

$$\mathcal{E}^{\text{Arrow}} = \{(c, n_\ell) \mid \ell = 1, \dots, N-1\}. \quad (21)$$

In Fig. 4, we provide an illustrative example of arrowhead RIS with $N = 5$ where port 1 is the central vertex. As a consequence, the susceptance matrix of arrowhead RIS is symmetric and arrowhead ($[\mathbf{B}]_{i,j} = 0$ if $i \neq c, j \neq c$, and $i \neq j$) [39]. Assuming port 1 is the central vertex, the susceptance matrix of arrowhead RIS can be written as

$$\mathbf{B} = \begin{bmatrix} [\mathbf{B}]_{1,1} & [\mathbf{B}]_{1,2} & \cdots & [\mathbf{B}]_{1,N} \\ [\mathbf{B}]_{1,2} & [\mathbf{B}]_{2,2} & \cdots & 0 \\ \vdots & \vdots & \ddots & \vdots \\ [\mathbf{B}]_{1,N} & 0 & \cdots & [\mathbf{B}]_{N,N} \end{bmatrix}. \quad (22)$$

Note that if the central vertex is not port 1, \mathbf{B} is a permuted arrowhead matrix.

It should be noted that all tree-connected RISs satisfy the necessary condition to be MISO optimal and contain the same number of tunable admittance components. Thus, tridiagonal and arrowhead RIS have the same circuit complexity and MISO optimality. In practice, we can select the suitable tree-connected RIS architecture according to the use case. On the one hand, tridiagonal RIS can be easily implemented with cables or tapes, thanks to the path graph circuit topology, so it enables the practical development of tree-connected RIS with uniform linear arrays (ULAs) or radio stripes [40]. In addition, tridiagonal RIS is the tree-connected architecture that minimizes the length of the interconnections since it connects only adjacent RIS elements. On the other hand, arrowhead BD-RIS is more suitable to develop tree-connected RIS with uniform planar arrays (UPAs).

C. Forest-Connected RIS

To further reduce the circuit complexity of tree-connected RIS, especially for the large-scale case, we propose forest-connected RIS. A forest-connected RIS is defined as a BD-RIS where the N RIS elements are divided into $G = N/N_G$ groups with group size N_G and each group utilizes the tree-connected architecture (i.e. the graph for each group is a tree on N_G vertices)⁴. Therefore, the graph \mathcal{G} associated with the forest-connected RIS is a forest, and the corresponding vertex and edge sets can be represented as

$$\mathcal{V} = \cup_{g=1}^G \mathcal{V}_g, \quad \mathcal{E} = \cup_{g=1}^G \mathcal{E}_g, \quad (23)$$

where \mathcal{V}_g and \mathcal{E}_g denote the vertex and edge sets of the graph associated with the g th group for $g = 1, \dots, G$, with $\mathcal{V}_{g_1} \cap \mathcal{V}_{g_2} = \emptyset$ for all $g_1 \neq g_2$.

More specifically, the tree-connected architecture for each group in the forest-connected RIS can be either tridiagonal or arrowhead. When the tridiagonal architecture is used, the

⁴Note that the tree-connected RIS is a special case of the forest-connected RIS, i.e., with $G = 1$. This is consistent with the fact that in graph theory a tree is a special case of forest.

vertex and edge sets of the graph associated with forest-connected RIS are defined as

$$\mathcal{V}_{\text{Forest}}^{\text{Tri}} = \cup_{g=1}^G \{n_{g,1}, n_{g,2}, \dots, n_{g,N_G}\}, \quad (24)$$

$$\mathcal{E}_{\text{Forest}}^{\text{Tri}} = \cup_{g=1}^G \{(n_{g,\ell}, n_{g,\ell+1}) \mid \ell = 1, \dots, N_G - 1\}, \quad (25)$$

similarly to (17) and (18). Accordingly, the susceptance matrix of forest-connected RIS with tridiagonal architecture for each group is block diagonal with each block being symmetric and tridiagonal. On the other hand, when the arrowhead architecture is used, the vertex and edge sets of the graph associated with forest-connected RIS are defined as

$$\mathcal{V}_{\text{Forest}}^{\text{Arrow}} = \cup_{g=1}^G \{c_g, n_{g,1}, n_{g,2}, \dots, n_{g,N_G-1}\}, \quad (26)$$

$$\mathcal{E}_{\text{Forest}}^{\text{Arrow}} = \cup_{g=1}^G \{(c_g, n_{g,\ell}) \mid \ell = 1, \dots, N_G - 1\}, \quad (27)$$

where c_g is the index of the central vertex for the g th group, similarly to (20) and (21). Accordingly, the susceptance matrix of forest-connected RIS with arrowhead architecture for each group is block diagonal with each block being symmetric and arrowhead.

The forest-connected RIS achieves a good performance-complexity trade-off between the single-connected and the tree-connected RIS. Note that the single-connected and tree-connected RIS can be viewed as two special cases of the forest-connected RIS, with $N_G = 1$ and $N_G = N$, respectively. In addition, forest-connected RIS is equivalent to group-connected RIS when $N_G = 2$ [4]. The number of tunable admittance components in forest-connected RIS with group size N_G is $N(2 - 1/N_G)$.

IV. OPTIMIZATION OF TREE- AND FOREST-CONNECTED RIS FOR MISO SYSTEMS

In this section, we optimize tree-connected and forest-connected RIS to maximize the received signal power in MISO systems. For tree-connected RIS, we show that any tree-connected RIS is MISO optimal and provide a closed-form global optimal solution. For forest-connected RIS, we provide a low-complexity iterative solution.

A. Tree-Connected RIS Optimization

The tree-connected RIS optimization to maximize the received signal power in MISO systems can be formulated as (10)-(14) plus a constraint that graph \mathcal{G} is a tree. Recall that the received signal power in BD-RIS-aided MISO systems is upper-bounded by $\bar{P}_R = P_T \|\mathbf{h}_{RI}\|^2 \|\mathbf{H}_{IT}\|^2$. In the following, we prove that there is always one and only one solution for the optimal susceptance matrix \mathbf{B} of tree-connected RIS to achieve the upper bound \bar{P}_R , and propose an algorithm to find such optimal \mathbf{B} .

Considering a RIS implemented through a reciprocal and lossless circuit, the key to achieving the upper bound \bar{P}_R given by (16) is to find a symmetric unitary matrix Θ satisfying

$$\hat{\mathbf{h}}_{RI}^H = \Theta \mathbf{u}_{IT}, \quad (28)$$

where $\hat{\mathbf{h}}_{RI} = \mathbf{h}_{RI} / \|\mathbf{h}_{RI}\|$ and $\mathbf{u}_{IT} = \mathbf{u}_{\max}(\mathbf{H}_{IT})$ is the dominant left singular vector of \mathbf{H}_{IT} ⁵. Substituting (3) into (28), we can equivalently rewrite (28) as

$$(\mathbf{I} + jZ_0\mathbf{B})\hat{\mathbf{h}}_{RI}^H = (\mathbf{I} - jZ_0\mathbf{B})\mathbf{u}_{IT}, \quad (29)$$

which can be expressed in a compact form as

$$\mathbf{B}\boldsymbol{\alpha} = \boldsymbol{\beta}, \quad (30)$$

where $\boldsymbol{\alpha} = jZ_0(\mathbf{u}_{IT} + \hat{\mathbf{h}}_{RI}^H) \in \mathbb{C}^{N \times 1}$ and $\boldsymbol{\beta} = \mathbf{u}_{IT} - \hat{\mathbf{h}}_{RI}^H \in \mathbb{C}^{N \times 1}$. The equation in (30) is composed of N linear equations with $2N - 1$ unknowns. The linear equation coefficients $\boldsymbol{\alpha}$ and $\boldsymbol{\beta}$ are complex vectors, while the $2N - 1$ unknowns are real since they are the entries of the susceptance matrix \mathbf{B} of the tree-connected RIS, which are not constrained to be zero as shown in (19) and (22). We aim to solve (30) as it is a sufficient and necessary condition to achieve the performance upper bound \bar{P}_R . To that end, we rewrite (30) as $2N$ equations with real coefficients and $2N - 1$ real unknowns, i.e.,

$$\begin{bmatrix} \mathbf{B} \\ -\bar{\mathbf{B}} \end{bmatrix} \mathbf{a} = \mathbf{b}, \quad (31)$$

where $\mathbf{a} \in \mathbb{R}^{2N \times 1}$ and $\mathbf{b} \in \mathbb{R}^{2N \times 1}$ are defined as

$$\mathbf{a} = \begin{bmatrix} \Re\{\boldsymbol{\alpha}\} \\ \Im\{\boldsymbol{\alpha}\} \end{bmatrix}, \quad \mathbf{b} = \begin{bmatrix} \Re\{\boldsymbol{\beta}\} \\ \Im\{\boldsymbol{\beta}\} \end{bmatrix}. \quad (32)$$

To solve (31), we further rewrite the equation such that the $2N - 1$ real unknowns are explicitly collected in a vector $\mathbf{x} \in \mathbb{R}^{(2N-1) \times 1}$. Specifically, given a tree-connected RIS whose graph has an edge set $\mathcal{E} = \{(n_\ell, m_\ell)\}_{\ell=1}^{N-1}$ such as (18) or (21), the $2N - 1$ real unknowns are collected as

$$\mathbf{x} = \left[[\mathbf{B}]_{1,1}, \dots, [\mathbf{B}]_{N,N}, [\mathbf{B}]_{n_1,m_1}, \dots, [\mathbf{B}]_{n_{N-1},m_{N-1}} \right]^T, \quad (33)$$

where $[\mathbf{B}]_{n,n}$ for $n = 1, \dots, N$ denote the N diagonal entries of \mathbf{B} and $[\mathbf{B}]_{n_\ell, m_\ell}$ for $\ell = 1, \dots, N - 1$ denote the $N - 1$ off-diagonal entries of \mathbf{B} specified by the edge set of graph. Accordingly, (31) can be equivalently rewritten as

$$\mathbf{A}\mathbf{x} = \mathbf{b}, \quad (34)$$

where $\mathbf{A} \in \mathbb{R}^{2N \times (2N-1)}$ is the coefficient matrix given by

$$\mathbf{A} = \begin{bmatrix} \Re\{\mathbf{A}_1\} & \Re\{\mathbf{A}_2\} \\ \Im\{\mathbf{A}_1\} & \Im\{\mathbf{A}_2\} \end{bmatrix}, \quad (35)$$

where $\mathbf{A}_1 \in \mathbb{C}^{N \times N}$ and $\mathbf{A}_2 \in \mathbb{C}^{N \times (N-1)}$. Because the real and imaginary parts of \mathbf{A}_1 are multiplied by the N diagonal entries of \mathbf{B} in (34), to build the equivalence between (31) and (34), \mathbf{A}_1 should be given by

$$\mathbf{A}_1 = \text{diag}(\boldsymbol{\alpha}). \quad (36)$$

On the other hand, the real and imaginary parts of \mathbf{A}_2 are multiplied by the $N - 1$ off-diagonal entries of \mathbf{B} including $[\mathbf{B}]_{n_1, m_1}, \dots, [\mathbf{B}]_{n_{N-1}, m_{N-1}}$. For this reason, the structure of

⁵Condition (28) is derived by considering $P_R \leq P_T \max_{\|\mathbf{x}\|=1} \|\mathbf{h}_{RI}\|^2 \|\Theta \mathbf{H}_{IT} \mathbf{x}\|^2 \leq P_T \max_{\|\mathbf{x}\|=1} \|\mathbf{h}_{RI}\|^2 \|\Theta \mathbf{H}_{IT}\|^2 \|\mathbf{x}\|^2$.

Note that the equality holds in the two inequalities when $\hat{\mathbf{h}}_{RI}^H$ is equal to the dominant left singular vector of $\Theta \mathbf{H}_{IT}$, i.e., $\Theta \mathbf{u}_{IT}$.

Algorithm 1 Closed-form global optimization of tree-connected RIS for MISO systems

Input: $\mathbf{h}_{RI} \in \mathbb{C}^{1 \times N}$, $\mathbf{H}_{IT} \in \mathbb{C}^{N \times M}$.

Output: \mathbf{B} .

- 1: Obtain $\hat{\mathbf{h}}_{RI} = \frac{\mathbf{h}_{RI}}{\|\mathbf{h}_{RI}\|}$, $\mathbf{u}_{IT} = \mathbf{u}_{\max}(\mathbf{H}_{IT})$.
 - 2: Obtain $\boldsymbol{\alpha} = jZ_0(\mathbf{u}_{IT} + \hat{\mathbf{h}}_{RI}^H)$, $\boldsymbol{\beta} = \mathbf{u}_{IT} - \hat{\mathbf{h}}_{RI}^H$.
 - 3: Obtain \mathbf{A}_1 and \mathbf{A}_2 by (36) and (37), respectively.
 - 4: Obtain \mathbf{A} and \mathbf{b} by (35) and (32), respectively.
 - 5: Obtain $\mathbf{x} = (\mathbf{A}^T \mathbf{A})^{-1} \mathbf{A}^T \mathbf{b}$.
 - 6: Obtain \mathbf{B} by (33).
-

\mathbf{A}_2 depends on how the RIS ports are connected to each other, that is the specific graph associated with the tree-connected RIS. Accordingly, the entry of the ℓ th column of \mathbf{A}_2 for $\ell = 1, \dots, N - 1$ is given by

$$[\mathbf{A}_2]_{k,\ell} = \begin{cases} [\boldsymbol{\alpha}]_{n_\ell} & \text{if } k = m_\ell \\ [\boldsymbol{\alpha}]_{m_\ell} & \text{if } k = n_\ell \\ 0 & \text{otherwise} \end{cases}. \quad (37)$$

Remarkably, the constraint on the tree-connected architecture, i.e., the position of the non-zero elements of \mathbf{B} , is dealt with by properly constructing \mathbf{A}_2 as in (37).

The following proposition provides a useful property of tree-connected RIS, which we can leverage to solve the linear equations (34).

Proposition 2. *For any tree-connected RIS with N elements, the coefficient matrix $\mathbf{A} \in \mathbb{R}^{2N \times (2N-1)}$ has full column rank, i.e., $r(\mathbf{A}) = 2N - 1$.*

Proof. Please refer to Appendix C. □

According to Proposition 2, the linear equations (34) has one solution or no solution [41]. Furthermore, we show that it has exactly one solution by using the following proposition.

Proposition 3. *For any tree-connected RIS with N elements, the augmented matrix $[\mathbf{A}|\mathbf{b}] \in \mathbb{R}^{2N \times 2N}$ has rank $r([\mathbf{A}|\mathbf{b}]) = 2N - 1$.*

Proof. Please refer to Appendix D. □

According to the Rouché-Capelli theorem [41], a system of linear equations is consistent if the rank of the coefficient matrix \mathbf{A} is equal to the rank of the augmented matrix $[\mathbf{A}|\mathbf{b}]$. Thus, according to Proposition 3, the system of linear equations (34) is consistent and has exactly one solution. As a result, we can find the solution of (34) as $\mathbf{x} = \mathbf{A}^\dagger \mathbf{b}$, where $\mathbf{A}^\dagger = (\mathbf{A}^T \mathbf{A})^{-1} \mathbf{A}^T$ is the Moore-Penrose pseudo-inverse of \mathbf{A} , and subsequently the optimal susceptance matrix \mathbf{B} of the tree-connected RIS can be found through (33).

To conclude, we prove that for any tree-connected RIS there is always one and only one global optimal solution for the susceptance matrix \mathbf{B} to achieve the upper bound \bar{P}_R for any channel realization. In Alg. 1, we summarize the steps required to optimize tree-connected RIS for MISO systems. Interestingly, Alg. 1 can be used to globally optimize tree-connected RISs in single-user multiple-input multiple-output

(MIMO) and multi-user MISO systems. More precisely, in single-user MIMO systems using single-stream transmission, the received signal power is maximized by applying Alg. 1 to the vectors \mathbf{v}_{RI} and \mathbf{u}_{IT} , with \mathbf{v}_{RI} being the dominant right singular vector of \mathbf{H}_{RI} . In addition, in multi-user MISO systems, the sum power is maximized by applying Alg. 1 to \mathbf{t}_{RI} and \mathbf{u}_{IT} , with \mathbf{t}_{RI} being the dominant right singular vector of $\mathbf{G}_{RI} = [\mathbf{h}_{RI,1}^H, \dots, \mathbf{h}_{RI,U}^H]^H$, where $\mathbf{h}_{RI,u} \in \mathbb{C}^{1 \times N}$ denotes the channel from the RIS to the u th receiver. The computational complexity of Alg. 1 is driven by the complexity of Step 5, i.e., it is the complexity of computing the inverse of $\mathbf{A}^T \mathbf{A}$. Since $\mathbf{A}^T \mathbf{A} \in \mathbb{R}^{(2N-1) \times (2N-1)}$, the computational complexity of Alg. 1 is $\mathcal{O}(8N^3)$.

B. Forest-Connected RIS Optimization

The forest-connected RIS optimization to maximize the received signal power in MISO systems is formulated as

$$\max_{\Theta, \mathbf{w}} P_T |\mathbf{h}_{RI} \Theta \mathbf{H}_{IT} \mathbf{w}|^2 \quad (38)$$

$$\text{s.t. } \Theta = (\mathbf{I} + jZ_0 \mathbf{B})^{-1} (\mathbf{I} - jZ_0 \mathbf{B}), \quad (39)$$

$$\mathbf{B} = \text{diag}(\mathbf{B}_1, \dots, \mathbf{B}_G), \quad (40)$$

$$\mathbf{B}_g = \mathbf{B}_g^T, \mathbf{B}_g \in \mathcal{B}_{\mathcal{G},g}, \forall g, \quad (41)$$

$$\|\mathbf{w}\| = 1, \quad (42)$$

where the susceptance matrix \mathbf{B} of the forest-connected RIS is a block diagonal matrix with \mathbf{B}_g being the g th block and $\mathcal{B}_{\mathcal{G},g}$ represents the set of the g th block written as

$$\mathcal{B}_{\mathcal{G},g} = \{\mathbf{B}_g | [\mathbf{B}_g]_{n,m} = 0, n \neq m, n, m \in \mathcal{V}_g, (n, m) \notin \mathcal{E}_g\}, \quad (43)$$

where \mathcal{V}_g and \mathcal{E}_g are the vertex and edge sets of the graph for the g th group for $g = 1, \dots, G$. Specifically, \mathcal{V}_g and \mathcal{E}_g can be found by (24) and (25) when the tridiagonal architecture is used for the g th group, or by (26) and (27) when the arrowhead architecture is used.

Different from optimizing the tree-connected RIS, it is hard to find a tight upper bound on the received signal power in forest-connected RIS-aided MISO systems due to block diagonal characteristics of the susceptance matrix, which makes it hard to derive a closed-form global optimal solution. To solve the challenging forest-connected RIS optimization problem, we propose an iterative approach, where the precoder \mathbf{w} and the RIS susceptance matrix \mathbf{B} are alternatively optimized.

1) *Optimizing \mathbf{B} with Fixed \mathbf{w}* : When the precoder \mathbf{w} is fixed, we introduce $\mathbf{h}_{IT}^{\text{eff}} = \mathbf{H}_{IT} \mathbf{w}$ as the effective channel between the transmitter and RIS so that the forest-connected RIS-aided MISO system is equivalently converted to a forest-connected RIS-aided SISO system. Thus, we can equivalently rewrite the problem (38)-(42) as

$$\max_{\Theta_g} P_T \left| \sum_{g=1}^G \mathbf{h}_{RI,g} \Theta_g \mathbf{h}_{IT,g}^{\text{eff}} \right|^2 \quad (44)$$

$$\text{s.t. } \Theta_g = (\mathbf{I} + jZ_0 \mathbf{B}_g)^{-1} (\mathbf{I} - jZ_0 \mathbf{B}_g), \quad (45)$$

$$\mathbf{B}_g = \mathbf{B}_g^T, \mathbf{B}_g \in \mathcal{B}_{\mathcal{G},g}, \forall g, \quad (46)$$

$$\|\mathbf{w}\| = 1, \quad (47)$$

Algorithm 2 Optimization of forest-connected RIS for MISO systems

Input: $\mathbf{h}_{RI} \in \mathbb{C}^{1 \times N}$, $\mathbf{H}_{IT} \in \mathbb{C}^{N \times M}$.

Output: \mathbf{B} and \mathbf{w} .

- 1: Initialize \mathbf{w} .
 - 2: **while** no convergence of objective (38) **do**
 - 3: Update \mathbf{B}_g by Alg. 1 with input $\mathbf{h}_{RI,g}$, $\mathbf{h}_{IT,g}^{\text{eff}}$, $\forall g$.
 - 4: Obtain Θ from $\mathbf{B} = \text{diag}(\mathbf{B}_1, \dots, \mathbf{B}_G)$ by (3).
 - 5: Update $\mathbf{w} = (\mathbf{h}_{RI} \Theta \mathbf{H}_{IT})^H / \|\mathbf{h}_{RI} \Theta \mathbf{H}_{IT}\|$.
 - 6: **end while**
-

where $\mathbf{h}_{RI,g} \in \mathbb{C}^{1 \times N_g}$ and $\mathbf{h}_{IT,g}^{\text{eff}} \in \mathbb{C}^{N_g \times 1}$ consist of the N_g entries of \mathbf{h}_{RI} and $\mathbf{h}_{IT}^{\text{eff}}$ corresponding to the RIS elements of the g th group, respectively [4]. To solve the problem (44)-(47), we first consider the case that the graph for each group is complete, that is the group-connected RIS where \mathbf{B}_g can be arbitrary symmetric matrix. As shown in [4] and [28], the received signal power in the group-connected RIS-aided SISO system, i.e. $P_T \left| \sum_{g=1}^G \mathbf{h}_{RI,g} \Theta_g \mathbf{h}_{IT,g}^{\text{eff}} \right|^2$, is upper bounded by

$$\bar{P}_R^{\text{eff}} = P_T \left(\sum_{g=1}^G \|\mathbf{h}_{RI,g}\| \|\mathbf{h}_{IT,g}^{\text{eff}}\| \right)^2. \quad (48)$$

The key to achieve such upper bound (48) is to find complex symmetric unitary matrices Θ_g for $g = 1, \dots, G$ satisfying

$$\hat{\mathbf{h}}_{RI,g}^H = \Theta_g \hat{\mathbf{h}}_{IT,g}^{\text{eff}}, \forall g, \quad (49)$$

where $\hat{\mathbf{h}}_{RI,g} = \mathbf{h}_{RI,g} / \|\mathbf{h}_{RI,g}\|$ and $\hat{\mathbf{h}}_{IT,g}^{\text{eff}} = \mathbf{h}_{IT,g}^{\text{eff}} / \|\mathbf{h}_{IT,g}^{\text{eff}}\|$. Recall that each group in the forest-connected RIS utilizes the tree-connected architecture. Thus, referring to the tree-connected RIS optimization shown in Section IV.A, it is straightforward to show that for each group of the forest-connected RIS there is always one and only one solution for \mathbf{B}_g whose corresponding Θ_g satisfying (49), so that the upper bound (48) can be achieved. Moreover, the optimal \mathbf{B}_g for each group can be found by Alg. 1 with the input of the channels $\mathbf{h}_{RI,g}$ and $\mathbf{h}_{IT,g}^{\text{eff}}$. Therefore, the susceptance matrix \mathbf{B} of the forest-connected RIS can be globally optimized to achieve the upper bound (48) when \mathbf{w} is fixed.

2) *Optimizing \mathbf{w} with Fixed \mathbf{B}* : When the RIS susceptance matrix \mathbf{B} is fixed, it is obvious that the optimal \mathbf{w} is the MRT given by $\mathbf{w} = (\mathbf{h}_{RI} \Theta \mathbf{H}_{IT})^H / \|\mathbf{h}_{RI} \Theta \mathbf{H}_{IT}\|$, where Θ can be computed by (3) as a function of \mathbf{B} .

The precoder \mathbf{w} and the RIS susceptance matrix \mathbf{B} are alternatively optimized until convergence of the objective (38). We summarize the steps to optimize forest-connected RIS in MISO systems in Alg. 2. The iterative algorithm is initialized by randomly setting \mathbf{w} to a feasible value. In addition, the convergence of Alg. 2 is guaranteed by the following two facts. First, at each iteration, the objective given by the received signal power P_R is non-decreasing. Second, the objective function is upper bounded by $P_T \|\mathbf{h}_{RI}\|^2 \|\mathbf{H}_{IT}\|^2$ because of the sub-multiplicativity of the spectral norm. The computational complexity per iteration of Alg. 2 is driven by the complexity

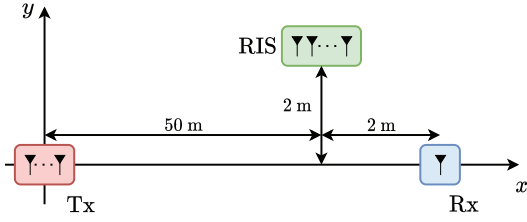


Fig. 5. Two-dimensional coordinate system for the RIS-aided MISO system.

of Step 3, i.e., it is the complexity of applying N/N_G times Alg. 1 to an N_G -element BD-RIS. Thus, the computational complexity per iteration of Alg. 2 is $\mathcal{O}(8NN_G^2)$.

V. PERFORMANCE EVALUATION

In this section, we provide the performance evaluation for the proposed tree- and forest-connected RIS. We consider a two-dimensional coordinate system, as shown in Fig. 5. The transmitter and receiver are located at $(0,0)$ and $(52,0)$ in meters (m), respectively. The RIS is located at $(50,2)$ and it is equipped with N elements. For the large-scale path loss, we use the distance-dependent path loss modeled as $L_{ij}(d_{ij}) = L_0(d_{ij}/D_0)^{-\alpha_{ij}}$, where L_0 is the reference path loss at distance $D_0 = 1$ m, d_{ij} is the distance, and α_{ij} is the path loss exponent for $ij \in \{RI, IT\}$. We set $L_0 = -30$ dB, $\alpha_{RI} = 2.8$, $\alpha_{IT} = 2$, and $P_T = 10$ mW. For the small-scale fading, we assume that the channel from the RIS to the receiver is Rayleigh fading. The channel from the transmitter to the RIS is modeled with Rician fading, given by

$$\mathbf{H}_{IT} = \sqrt{L_{IT}} \left(\sqrt{\frac{K}{1+K}} \mathbf{H}_{IT}^{\text{LoS}} + \sqrt{\frac{1}{1+K}} \mathbf{H}_{IT}^{\text{NLoS}} \right), \quad (50)$$

where K refers to the Rician factor, while $\mathbf{H}_{IT}^{\text{LoS}}$ and $\text{vec}(\mathbf{H}_{IT}^{\text{NLoS}}) \sim \mathcal{CN}(\mathbf{0}, \mathbf{I})$ represent the small-scale line-of-sight (LoS) and non-line-of-sight (NLoS) (Rayleigh fading) components, respectively. We consider two scenarios, with Rician factor $K = 0$ dB and $K = 10$ dB.

A. Tree-Connected RIS-Aided MISO Systems

We first evaluate the performance of the tree-connected RIS to verify that it is MISO optimal. Specifically, the tree-connected RIS is optimized through Alg. 1 and compared with the performance upper bound (16) achieved by the fully-connected RIS. We recall that in the fully-connected RIS, all the RIS ports are connected with each other, so that \mathbf{B} is an arbitrary symmetric matrix and Θ satisfies that

$$\Theta^H \Theta = \mathbf{I}, \Theta = \Theta^T, \quad (51)$$

as shown in [4]. In Fig. 6, we provide the received signal power achieved in MISO systems aided by fully- and tree-connected RIS. We can make the following observations. *First*, as expected, the tree-connected RIS can always achieve the performance upper bound. However, it has much lower circuit complexity than the fully-connected RIS, which will be quantitatively shown in Section V-C. *Second*, higher received signal

power can be obtained by increasing the number of transmit antennas M for both fully- and tree-connected RIS. *Last*, Rician fading channels with a lower Rician factor offer richer scattering, allowing to reach a slightly higher performance.

B. Forest-Connected RIS-Aided MISO Systems

We next evaluate the performance of the forest-connected RIS. Specifically, the forest-connected RIS is optimized through Alg. 2 and it is compared with tree-, group-, and single-connected RIS. For the group-connected RIS, we recall that the N elements are divided into G groups and all the RIS ports within the same group are connected with each other, so that \mathbf{B} is a symmetric block diagonal matrix and Θ satisfies

$$\Theta = \text{diag}(\Theta_1, \Theta_2, \dots, \Theta_G), \quad (52)$$

$$\Theta_g = \Theta_g^T, \Theta_g^H \Theta_g = \mathbf{I}, \forall g, \quad (53)$$

as shown in [4]. In Figs. 7 and 8, we provide the received signal power in MISO systems aided by tree-, group-, forest-, and single-connected RIS, with $M = 2$ and $M = 8$, respectively. Group-connected and single-connected RIS are optimized as proposed in [28, Alg. 2]. We can make the following observations.

First, the forest-connected RIS can always achieve the same received signal power as the group-connected RIS with the same group size. However, it has a much lower circuit complexity than the group-connected RIS with the same group size, as quantitatively shown in Section V-C.

Second, the forest-connected RIS achieves a higher received signal power than the single-connected RIS. For example, forest-connected RIS with group size 8 brings an improvement in the received signal power of 44.6%, when $M = 2$, $N = 64$, and $K = 0$ dB. On the other hand, it achieves a lower received signal power than the tree-connected RIS due to the simplified circuit complexity. Therefore, it is shown that the forest-connected RIS achieves a good performance-complexity trade-off between the single- and tree-connected RIS.

Third, the received signal power increases with the group size in the forest-connected RIS, which is because increasing the group size can provide more flexibility to the BD-RIS.

Fourth, higher received signal power can be obtained by increasing the number of transmit antennas M .

Last, BD-RIS is particularly beneficial over single-connected RIS in the presence of fading channels with lower Rician factors, in agreement with [4].

In Fig. 9, we also provide the achievable rate in MISO systems aided by tree-, group-, forest-, and single-connected RIS, with $M = 2$, $K = 0$ dB, and AWGN power $\sigma^2 = -80$ dBm. With $N = 64$, the tree-connected RIS improves the achievable rate by 10% over the single-connected RIS. In addition, the performance of a 64-element single-connected RIS can be obtained by a 52-element tree-connected RIS, which is beneficial for reducing by 19% the area of RIS.

C. Circuit Topology Complexity

We finally evaluate the circuit topology complexity of the proposed tree- and forest-connected RIS. As analyzed in

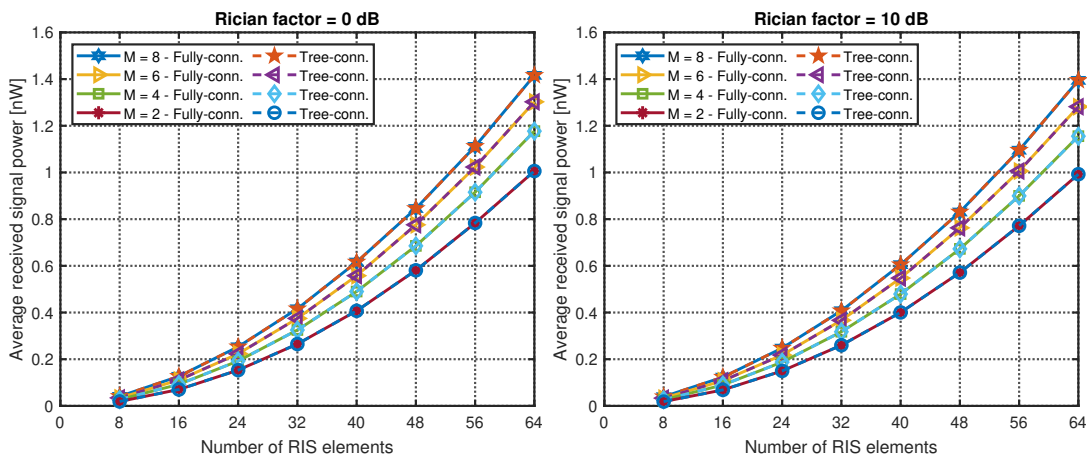


Fig. 6. Received signal power in MISO systems aided by fully- and tree-connected RIS.

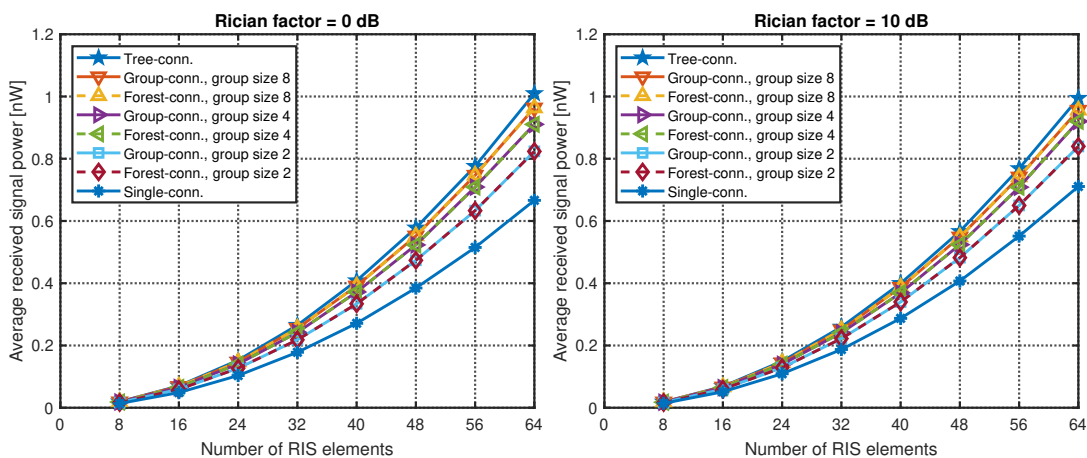


Fig. 7. Received signal power in MISO systems aided by tree-, group-, forest-, and single-connected RIS, with $M = 2$.

Section III, the circuit topology complexity in terms of the number of the tunable admittance components of the tree- and forest-connected RIS is $2N - 1$ and $N(2 - 1/N_G)$, respectively. For comparison, we also consider the circuit topology complexity of fully-, group-, and single-connected RIS, given by $N(N+1)/2$, $N(N_G+1)/2$, and N , respectively [4]. In Fig. 10, we provide the number of tunable admittance components in the fully-, group, tree-, forest-, and single-connected RIS. We can make the following observations.

First, compared with the fully-connected RIS, the tree-connected RIS has much lower circuit topology complexity. For example, the number of tunable admittance components is decreased by 16.4 times when $N = 64$ in the tree-connected RIS compared to the fully-connected RIS, but they achieve the same performance.

Second, compared with the group-connected RIS with same group size, the forest-connected RIS has much lower circuit topology complexity. For example, the number of tunable admittance components is reduced by 2.4 times when $N = 64$ in the forest-connected RIS compared to the group-connected RIS with group size 8, but they achieve the same performance.

Third, increasing the group size in the forest-connected RIS will increase the number of tunable admittance components while also enhancing the performance.

Fourth, compared with the single-connected RIS, the tree- and forest-connected RIS introduce appropriate complexity but achieves an improvement in the received power.

To conclude, we demonstrate that the benefit of the tree-connected (resp. forest-connected) RIS over the fully-connected (resp. group-connected) RIS lies in their highly simplified circuit complexity while maintaining optimal performance. Therefore, the proposed tree- and forest-connected architectures significantly improve the performance-complexity trade-off over existing BD-RIS architectures.

VI. CONCLUSION

We propose novel modeling, architecture design, and optimization for BD-RIS by utilizing graph theory. In particular, we model BD-RIS architectures as graphs, capturing the presence of interconnections between the RIS elements. Through this modeling, we prove that a BD-RIS achieves the performance upper bound in MISO systems if and only if its associated graph is connected. This remarkable result allows us to characterize the least complex BD-RIS architectures able to achieve the performance upper bound in MISO systems, denoted as tree-connected RIS. We also propose forest-connected RIS to bridge between the single-connected and the

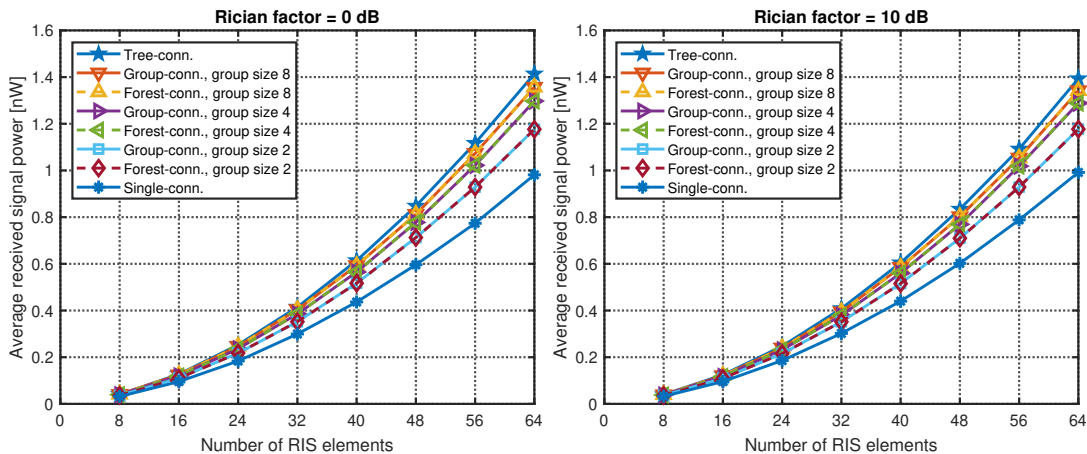


Fig. 8. Received signal power in MISO systems aided by tree-, group-, forest-, and single-connected RIS, with $M = 8$.

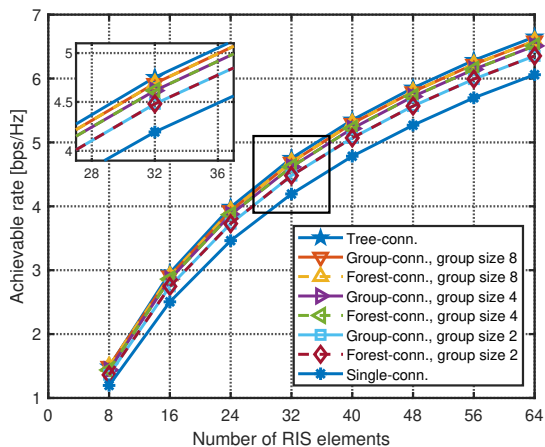


Fig. 9. Achievable rate in MISO systems aided by tree-, group-, forest-, and single-connected RIS, with $M = 2$ and $K = 0$ dB.

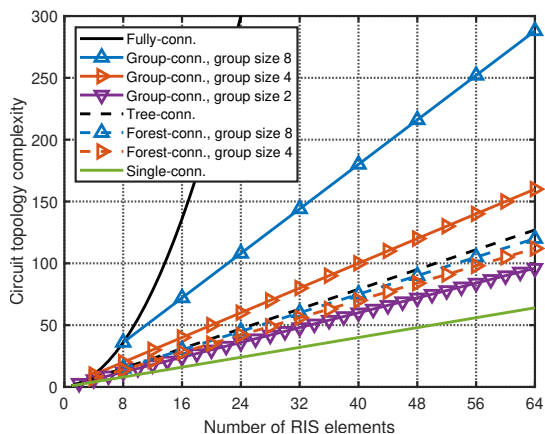


Fig. 10. Circuit topology complexity, i.e., the number of tunable admittance components, of fully-, group-, tree-, forest-, and single-connected RIS.

tree-connected architectures. To optimize these novel BD-RIS architectures, we derive a closed-form global optimal solution for tree-connected RIS, and an iterative algorithm for forest-connected RIS. Numerical results confirm that tree-connected (resp. forest-connected) RIS achieve the same performance

as fully-connected (resp. group-connected) RIS, with a significantly reduced circuit complexity by up to 16.4 times. We leave the optimization and performance evaluation of the proposed tree- and forest-connected RISs in other scenarios such as multi-user systems as the object of future research.

The proposed graph theoretical modeling of BD-RIS is expected to promote significant advancements in the growth of BD-RIS. This modeling can be used to explore the vast design space of possible architectures and evaluate them in terms of achievable performance and circuit complexity. This will enable the systematic development of new BD-RIS architectures with a more favorable balance between performance and complexity, and the implementation of BD-RIS prototypes.

APPENDIX

A. Proof of Lemma 1

We prove the necessary condition by showing that if \mathcal{G} is not a connected graph, the corresponding BD-RIS is not MISO optimal. If \mathcal{G} is disconnected, it has $C \geq 2$ connected components, where the c th component includes $N^{(c)}$ ports, for $c = 1, \dots, C$, with $\sum_{c=1}^C N^{(c)} = N$. With no loss of generality, we assume that each component includes adjacent ports. Thus, the admittance matrix \mathbf{Y} given by (6) is block diagonal, with the c th block having dimensions $N^{(c)} \times N^{(c)}$, for $c = 1, \dots, C$. As a consequence of (2), also the scattering matrix Θ is block diagonal, and writes as $\Theta = \text{diag}(\Theta_1, \dots, \Theta_C)$, where $\Theta_c \in \mathbb{C}^{N^{(c)} \times N^{(c)}}$, for $c = 1, \dots, C$. Thus, the received signal power (10) in the case of a disconnected graph \mathcal{G} is

$$P_R^{\text{DisC}} = P_T \left| \sum_{c=1}^C \mathbf{h}_{RI,c} \Theta_c \mathbf{H}_{IT,c} \mathbf{w} \right|^2, \quad (54)$$

where $\mathbf{h}_{RI,c} \in \mathbb{C}^{1 \times N^{(c)}}$ and $\mathbf{H}_{IT,c} \in \mathbb{C}^{N^{(c)} \times M}$ contain the $N^{(c)}$ elements of \mathbf{h}_{RI} and rows of \mathbf{H}_{IT} corresponding to the $N^{(c)}$ RIS elements grouped into the c th component, respectively. The received signal power P_R^{DisC} is upper bounded by

$$\bar{P}_R^{\text{DisC}} = P_T \left(\sum_{c=1}^C \|\mathbf{h}_{RI,c}\| \|\mathbf{H}_{IT,c} \mathbf{w}\| \right)^2, \quad (55)$$

following the Cauchy-Schwarz inequality and that $\Theta_c^H \Theta_c = \mathbf{I}$, for $c = 1, \dots, C$. Furthermore, it holds that

$$\bar{P}_R^{\text{DisC}} \stackrel{(a)}{\leq} P_T \|\mathbf{h}_{RI}\|^2 \|\mathbf{H}_{IT} \mathbf{w}\|^2 \stackrel{(b)}{\leq} \bar{P}_R, \quad (56)$$

where (a) follows by the Cauchy-Schwarz inequality and (b) follows by the definition of the spectral norm. Note that (b) is an equality if and only if \mathbf{w} is the dominant right singular vector of \mathbf{H}_{IT} . However, (a) is in general a strict inequality if \mathbf{w} is the dominant right singular vector of \mathbf{H}_{IT} , which thus proves the necessary condition of the lemma.

On the other hand, we prove the sufficient condition by showing that if \mathcal{G} is a connected graph, the corresponding BD-RIS is MISO optimal. This is straightforward to prove because 1) for a connected graph, we can always remove some edges to make it a tree, i.e. setting the corresponding off-diagonal entries of \mathbf{B} zero, 2) there exist one and only one solution for any RIS whose associated graph is a tree to achieve the performance upper bound (i.e., to be MISO optimal) as shown in Section IV. A.

B. Proof of Proposition 1

Applying Lemma 1, we need to prove that a connected graph with N vertices has at least $N-1$ edges. This is achieved by induction. The base case is easily verified: a connected graph with a single vertex has at least zero edges. As the induction step, we consider a connected graph with N vertices. From this graph, we remove edges (at least one) until we obtain a disconnected graph with two connected components. Assuming the two components have K and $N-K$ vertices, they have at least $K-1$ and $N-K-1$ edges by the induction hypothesis, respectively. Since we removed at least one edge to disconnect the graph, it had originally at least $(K-1) + (N-K-1) + 1 = N-1$ edges.

C. Proof of Proposition 2

This proof is conducted by induction. As the base case, we consider the only tree-connected RIS that can be realized with $N=2$ ports. This RIS includes two tunable admittance components connecting the two ports to ground and a further tunable admittance connecting the two ports to each other.

Based on the susceptance matrix $\mathbf{B} \in \mathbb{R}^{2 \times 2}$, the left-hand side of the system (34) is built by setting $\mathbf{x} = [[\mathbf{B}]_{1,1}, [\mathbf{B}]_{2,2}, [\mathbf{B}]_{1,2}]^T$. Accordingly, $\mathbf{A} \in \mathbb{R}^{4 \times 3}$ is given by (35) with $\mathbf{A}_1 \in \mathbb{C}^{2 \times 2}$ as in (36) and $\mathbf{A}_2 \in \mathbb{C}^{2 \times 1}$ given by $\mathbf{A}_2 = [[\alpha]_2, [\alpha]_1]^T$. Thus, it is easy to recognize that \mathbf{A} has in general full column rank, i.e., $r(\mathbf{A}) = 3$. The proposition is hence verified for the case $N=2$.

As the induction step, we prove that if the proposition is valid for RISs with $N-1$ ports, it also holds for RISs with N ports. We consider a tree-connected RIS with $N-1$ elements, whose coefficient matrix is given by

$$\mathbf{A}^{(N-1)} = \left[\begin{array}{c|c} \Re \left\{ \mathbf{A}_1^{(N-1)} \right\} & \Re \left\{ \mathbf{A}_2^{(N-1)} \right\} \\ \hline \Im \left\{ \mathbf{A}_1^{(N-1)} \right\} & \Im \left\{ \mathbf{A}_2^{(N-1)} \right\} \end{array} \right]. \quad (57)$$

To this $(N-1)$ -port tree-connected RIS, we connect an additional port creating an N -port tree-connected RIS. With

no loss of generality, we assume that the additional port is connected to the $(N-1)$ th port through a tunable admittance. In this way, the resulting N -port BD-RIS has the coefficient matrix

$$\mathbf{A}^{(N)} = \left[\begin{array}{c|c} \Re \left\{ \mathbf{A}_1^{(N)} \right\} & \Re \left\{ \mathbf{A}_2^{(N)} \right\} \\ \hline \Im \left\{ \mathbf{A}_1^{(N)} \right\} & \Im \left\{ \mathbf{A}_2^{(N)} \right\} \end{array} \right], \quad (58)$$

where $\mathbf{A}_1^{(N)} \in \mathbb{C}^{N \times N}$ and $\mathbf{A}_2^{(N)} \in \mathbb{C}^{N \times (N-1)}$ are given by

$$\mathbf{A}_1^{(N)} = \left[\begin{array}{c|c} \mathbf{A}_1^{(N-1)} & \mathbf{0}_{(N-1) \times 1} \\ \hline \mathbf{0}_{1 \times (N-1)} & [\alpha]_N \end{array} \right], \quad (59)$$

$$\mathbf{A}_2^{(N)} = \left[\begin{array}{c|c} \mathbf{A}_2^{(N-1)} & \mathbf{0}_{(N-2) \times 1} \\ \hline \mathbf{0}_{1 \times (N-2)} & [\alpha]_{N-1} \end{array} \right], \quad (60)$$

with $\mathbf{0}_{R \times C}$ denoting an $R \times C$ all-zero matrix. To prove the induction step, we need to show that $r(\mathbf{A}^{(N-1)}) = 2(N-1) - 1$ implies $r(\mathbf{A}^{(N)}) = 2N - 1$. To this end, $\mathbf{A}^{(N)}$ is rewritten as

$$\mathbf{A}^{(N)} \sim \left[\begin{array}{cc|c} \mathbf{A}^{(N-1)} & \mathbf{0}_{(2N-2) \times 1} & \begin{array}{c} \mathbf{0}_{(N-2) \times 1} \\ \Re \{ [\alpha]_N \} \\ \mathbf{0}_{(N-2) \times 1} \\ \Im \{ [\alpha]_N \} \end{array} \\ \hline \mathbf{0}_{2 \times (2N-3)} & \begin{array}{c} \Re \{ [\alpha]_N \} \\ \Im \{ [\alpha]_N \} \end{array} & \begin{array}{c} \Re \{ [\alpha]_{N-1} \} \\ \Im \{ [\alpha]_{N-1} \} \end{array} \end{array} \right], \quad (61)$$

by applying appropriate row and column swapping operations. From (61), we notice that if $\mathbf{A}^{(N-1)}$ has full column rank and the vectors $[\Re \{ [\alpha]_N \}, \Im \{ [\alpha]_N \}]$ and $[\Re \{ [\alpha]_{N-1} \}, \Im \{ [\alpha]_{N-1} \}]$ are linearly independent, then $\mathbf{A}^{(N)}$ has full column rank. Since $[\Re \{ [\alpha]_N \}, \Im \{ [\alpha]_N \}]$ and $[\Re \{ [\alpha]_{N-1} \}, \Im \{ [\alpha]_{N-1} \}]$ are in practice linearly independent with probability 1, the induction step is proven.

D. Proof of Proposition 3

To prove that $r([\mathbf{A}|\mathbf{b}]) = 2N - 1$, we show that it is always possible to obtain a zero row in $[\mathbf{A}|\mathbf{b}]$ by applying appropriate row operations. Firstly, we execute on $[\mathbf{A}|\mathbf{b}]$ the N row operations

$$\mathbf{r}_{N+n} = \mathbf{r}_{N+n} - \frac{\Im \{ [\alpha]_n \}}{\Re \{ [\alpha]_n \}} \mathbf{r}_n, \quad (62)$$

for $n = 1, \dots, N$, where \mathbf{r}_n denotes the n th row of $[\mathbf{A}|\mathbf{b}]$. The resulting matrix is given by

$$[\mathbf{A}|\mathbf{b}] \sim \left[\begin{array}{c|c|c} \Re \left\{ \mathbf{A}_1 \right\} & \Re \left\{ \mathbf{A}_2 \right\} & \Re \left\{ \beta \right\} \\ \hline \mathbf{0}_{N \times N} & \mathbf{A}' & \mathbf{b}' \end{array} \right], \quad (63)$$

where we introduced $\mathbf{A}' \in \mathbb{R}^{N \times (N-1)}$ and $\mathbf{b}' \in \mathbb{R}^{N \times 1}$. The matrix \mathbf{A}' has exactly two non-zero elements in each column, in the same positions as the non-zero elements in \mathbf{A}_2 . Specifically,

$$\begin{cases} [\mathbf{A}']_{n_\ell, \ell} &= \Im \{ [\alpha]_{m_\ell} \} - \frac{\Im \{ [\alpha]_{n_\ell} \}}{\Re \{ [\alpha]_{n_\ell} \}} \Re \{ [\alpha]_{m_\ell} \}, \\ [\mathbf{A}']_{m_\ell, \ell} &= \Im \{ [\alpha]_{n_\ell} \} - \frac{\Im \{ [\alpha]_{m_\ell} \}}{\Re \{ [\alpha]_{m_\ell} \}} \Re \{ [\alpha]_{n_\ell} \}, \\ [\mathbf{A}']_{p, \ell} &= 0, \forall p \neq m_\ell, n_\ell, \end{cases} \quad (64)$$

for $\ell = 1, \dots, N-1$, with n_ℓ and m_ℓ being the row indexes of the two non-zero elements in the ℓ th column of \mathbf{A}_2 . The vector \mathbf{b}' writes as

$$[\mathbf{b}']_n = \Im \{[\boldsymbol{\beta}]_n\} - \frac{\Re \{[\boldsymbol{\alpha}]_n\}}{\Re \{[\boldsymbol{\alpha}]_n\}} \Re \{[\boldsymbol{\beta}]_n\}, \quad (65)$$

for $n = 1, \dots, N$. Secondly, we execute on the resulting $[\mathbf{A}|\mathbf{b}]$ the N row operations

$$\mathbf{r}_{N+n} = \Re \{[\boldsymbol{\alpha}]_n\} \mathbf{r}_{N+n}, \quad (66)$$

for $n = 1, \dots, N$, followed by the $N-1$ row operations

$$\mathbf{r}_{2N} = \mathbf{r}_{2N} + \mathbf{r}_{N+n}, \quad (67)$$

for $n = 1, \dots, N-1$. The resulting matrix is given by

$$[\mathbf{A}|\mathbf{b}] \sim \begin{bmatrix} \Re \{\mathbf{A}_1\} & \Re \{\mathbf{A}_2\} & \Re \{\boldsymbol{\beta}\} \\ \mathbf{0}_{N \times N} & \mathbf{A}'' & \mathbf{b}'' \end{bmatrix}, \quad (68)$$

where we introduced $\mathbf{A}'' \in \mathbb{R}^{N \times N-1}$ and $\mathbf{b}'' \in \mathbb{R}^{N \times 1}$.

We now show that (68) has rank $2N-1$ since its $2N$ th row is all-zero. To this end, we need to prove that $[\mathbf{A}'']_{N,\ell} = 0$, for $\ell = 1, \dots, N-1$, and that $[\mathbf{b}'']_N = 0$. Indeed, we have

$$[\mathbf{A}'']_{N,\ell} = \Re \{[\boldsymbol{\alpha}]_{n_\ell}\} [\mathbf{A}']_{n_\ell,\ell} + \Re \{[\boldsymbol{\alpha}]_{m_\ell}\} [\mathbf{A}']_{m_\ell,\ell} = 0 \quad (69)$$

for $\ell = 1, \dots, N-1$, with n_ℓ and m_ℓ being the row indexes of the two non-zero elements in the ℓ th column of \mathbf{A}_2 . Furthermore, the N th entry of vector \mathbf{b}'' is given by

$$\begin{aligned} [\mathbf{b}'']_N &= \sum_{n=1}^N \Re \{[\boldsymbol{\alpha}]_n\} [\mathbf{b}']_n \\ &= \sum_{n=1}^N \Re \{[\boldsymbol{\alpha}]_n\} \Im \{[\boldsymbol{\beta}]_n\} - \Im \{[\boldsymbol{\alpha}]_n\} \Re \{[\boldsymbol{\beta}]_n\}, \end{aligned} \quad (70)$$

where

$$\Re \{[\boldsymbol{\alpha}]_n\} \Im \{[\boldsymbol{\beta}]_n\} - \Im \{[\boldsymbol{\alpha}]_n\} \Re \{[\boldsymbol{\beta}]_n\} \quad (72)$$

$$= jZ_0 \left(\Im \left\{ \left[\hat{\mathbf{h}}_{RI}^H \right]_n \right\}^2 - \Im \{[\mathbf{u}_{IT}]_n\}^2 \right) \quad (73)$$

$$+ \Re \left\{ \left[\hat{\mathbf{h}}_{RI}^H \right]_n \right\}^2 - \Re \{[\mathbf{u}_{IT}]_n\}^2 \right) \quad (74)$$

$$= jZ_0 \left(\left| \left[\hat{\mathbf{h}}_{RI}^H \right]_n \right|^2 - \|\mathbf{u}_{IT}\|_n^2 \right). \quad (75)$$

Thus, recalling that $\|\hat{\mathbf{h}}_{RI}^H\|^2 = 1$ and $\|\mathbf{u}_{IT}\|^2 = 1$, we have

$$[\mathbf{b}'']_N = jZ_0 \left(\left| \left[\hat{\mathbf{h}}_{RI}^H \right]_N \right|^2 - \|\mathbf{u}_{IT}\|^2 \right) = 0, \quad (76)$$

proving that the $2N$ th row of (68) is all-zero.

REFERENCES

- [1] E. Basar, M. Di Renzo, J. De Rosny, M. Debbah, M.-S. Alouini, and R. Zhang, "Wireless Communications Through Reconfigurable Intelligent Surfaces," *IEEE Access*, vol. 7, pp. 116753–116773, 2019.
- [2] Q. Wu and R. Zhang, "Towards Smart and Reconfigurable Environment: Intelligent Reflecting Surface Aided Wireless Network," *IEEE Commun. Mag.*, vol. 58, no. 1, pp. 106–112, 2020.
- [3] Q. Wu, S. Zhang, B. Zheng, C. You, and R. Zhang, "Intelligent Reflecting Surface-Aided Wireless Communications: A Tutorial," *IEEE Trans. Commun.*, vol. 69, no. 5, pp. 3313–3351, 2021.
- [4] S. Shen, B. Clerckx, and R. Murch, "Modeling and Architecture Design of Reconfigurable Intelligent Surfaces Using Scattering Parameter Network Analysis," *IEEE Trans. Wireless Commun.*, pp. 1–1, 2021.
- [5] Q. Wu and R. Zhang, "Intelligent reflecting surface enhanced wireless network via joint active and passive beamforming," *IEEE Trans. Wireless Commun.*, vol. 18, no. 11, pp. 5394–5409, 2019.
- [6] H. Guo, Y.-C. Liang, J. Chen, and E. G. Larsson, "Weighted sum-rate maximization for reconfigurable intelligent surface aided wireless networks," *IEEE Trans. Wireless Commun.*, vol. 19, no. 5, pp. 3064–3076, 2020.
- [7] Y. Liu, J. Zhao, M. Li, and Q. Wu, "Intelligent reflecting surface aided MISO uplink communication network: Feasibility and power minimization for perfect and imperfect CSI," *IEEE Trans. Commun.*, vol. 69, no. 3, pp. 1975–1989, 2021.
- [8] C. Pan, H. Ren, K. Wang, W. Xu, M. El-kashlan, A. Nallanathan, and L. Hanzo, "Multicell MIMO communications relying on intelligent reflecting surfaces," *IEEE Trans. Wireless Commun.*, vol. 19, no. 8, pp. 5218–5233, 2020.
- [9] H. Li, W. Cai, Y. Liu, M. Li, Q. Liu, and Q. Wu, "Intelligent reflecting surface enhanced wideband MIMO-OFDM communications: From practical model to reflection optimization," *IEEE Trans. Commun.*, vol. 69, no. 7, pp. 4807–4820, 2021.
- [10] Y. Xiu, J. Zhao, W. Sun, M. D. Renzo, G. Gui, Z. Zhang, and N. Wei, "Reconfigurable intelligent surfaces aided mmwave NOMA: Joint power allocation, phase shifts, and hybrid beamforming optimization," *IEEE Trans. Wireless Commun.*, vol. 20, no. 12, pp. 8393–8409, 2021.
- [11] A. Bansal, K. Singh, B. Clerckx, C.-P. Li, and M.-S. Alouini, "Rate-splitting multiple access for intelligent reflecting surface aided multi-user communications," *IEEE Trans. Veh. Technol.*, vol. 70, no. 9, pp. 9217–9229, 2021.
- [12] J. Hu, H. Zhang, B. Di, L. Li, K. Bian, L. Song, Y. Li, Z. Han, and H. V. Poor, "Reconfigurable intelligent surface based RF sensing: Design, optimization, and implementation," *IEEE J. Sel. Areas Commun.*, vol. 38, no. 11, pp. 2700–2716, 2020.
- [13] Z. Feng, B. Clerckx, and Y. Zhao, "Waveform and beamforming design for intelligent reflecting surface aided wireless power transfer: Single-user and multi-user solutions," *IEEE Trans. Wireless Commun.*, vol. 21, no. 7, pp. 5346–5361, 2022.
- [14] Y. Zhao, B. Clerckx, and Z. Feng, "IRS-aided SWIPT: Joint waveform, active and passive beamforming design under nonlinear harvester model," *IEEE Trans. Commun.*, vol. 70, no. 2, pp. 1345–1359, 2022.
- [15] Z. Peng, Z. Chen, C. Pan, G. Zhou, and H. Ren, "Robust transmission design for RIS-aided communications with both transceiver hardware impairments and imperfect CSI," *IEEE Wireless Commun. Lett.*, vol. 11, no. 3, pp. 528–532, 2022.
- [16] Y. Chen, Y. Wang, and L. Jiao, "Robust transmission for reconfigurable intelligent surface aided millimeter wave vehicular communications with statistical CSI," *IEEE Trans. Wireless Commun.*, vol. 21, no. 2, pp. 928–944, 2022.
- [17] B. Zheng, C. You, and R. Zhang, "Double-IRS assisted multi-user MIMO: Cooperative passive beamforming design," *IEEE Trans. Wireless Commun.*, vol. 20, no. 7, pp. 4513–4526, 2021.
- [18] W. Mei and R. Zhang, "Intelligent reflecting surface for multi-path beam routing with active/passive beam splitting and combining," *IEEE Commun. Lett.*, vol. 26, no. 5, pp. 1165–1169, 2022.
- [19] Q. Wu and R. Zhang, "Beamforming optimization for intelligent reflecting surface with discrete phase shifts," in *ICASSP 2019 - 2019 IEEE International Conference on Acoustics, Speech and Signal Processing (ICASSP)*, 2019, pp. 7830–7833.
- [20] B. Di, H. Zhang, L. Song, Y. Li, Z. Han, and H. V. Poor, "Hybrid beamforming for reconfigurable intelligent surface based multi-user communications: Achievable rates with limited discrete phase shifts," *IEEE J. Sel. Areas Commun.*, vol. 38, no. 8, pp. 1809–1822, 2020.
- [21] H. Guo and V. K. N. Lau, "Uplink cascaded channel estimation for intelligent reflecting surface assisted multiuser MISO systems," *IEEE Trans. Signal Process.*, vol. 70, pp. 3964–3977, 2022.
- [22] R. Long, Y.-C. Liang, Y. Pei, and E. G. Larsson, "Active reconfigurable intelligent surface-aided wireless communications," *IEEE Trans. Wireless Commun.*, vol. 20, no. 8, pp. 4962–4975, 2021.
- [23] Z. Zhang, L. Dai, X. Chen, C. Liu, F. Yang, R. Schober, and H. V. Poor, "Active RIS vs. passive RIS: Which will prevail in 6G?" *IEEE Trans. Commun.*, vol. 71, no. 3, pp. 1707–1725, 2023.
- [24] L. Dai, B. Wang, M. Wang, X. Yang, J. Tan, S. Bi, S. Xu, F. Yang, Z. Chen, M. D. Renzo, C.-B. Chae, and L. Hanzo, "Reconfigurable intelligent surface-based wireless communications: Antenna design, prototyping, and experimental results," *IEEE Access*, vol. 8, pp. 45913–45923, 2020.

- [25] J. Rao, Y. Zhang, S. Tang, Z. Li, S. Shen, C.-Y. Chiu, and R. Murch, "A novel reconfigurable intelligent surface for wide-angle passive beam-forming," *IEEE Trans. Microw. Theory Tech.*, vol. 70, no. 12, pp. 5427–5439, 2022.
- [26] H. Li, S. Shen, M. Nerini, and B. Clerckx, "Reconfigurable intelligent surfaces 2.0: Beyond diagonal phase shift matrices," *IEEE Commun. Mag.*, pp. 1–7, 2023.
- [27] M. Nerini, S. Shen, and B. Clerckx, "Discrete-value group and fully connected architectures for beyond diagonal reconfigurable intelligent surfaces," *IEEE Trans. Veh. Technol.*, pp. 1–15, 2023.
- [28] —, "Closed-form global optimization of beyond diagonal reconfigurable intelligent surfaces," *IEEE Trans. Wireless Commun.*, pp. 1–1, 2023.
- [29] J. Xu, Y. Liu, X. Mu, and O. A. Dobre, "STAR-RISs: Simultaneous transmitting and reflecting reconfigurable intelligent surfaces," *IEEE Commun. Lett.*, vol. 25, no. 9, pp. 3134–3138, 2021.
- [30] H. Zhang, S. Zeng, B. Di, Y. Tan, M. Di Renzo, M. Debbah, Z. Han, H. V. Poor, and L. Song, "Intelligent omni-surfaces for full-dimensional wireless communications: Principles, technology, and implementation," *IEEE Commun. Mag.*, vol. 60, no. 2, pp. 39–45, 2022.
- [31] H. Li, S. Shen, and B. Clerckx, "Beyond diagonal reconfigurable intelligent surfaces: From transmitting and reflecting modes to single-, group-, and fully-connected architectures," *IEEE Trans. Wireless Commun.*, vol. 22, no. 4, pp. 2311–2324, 2023.
- [32] —, "Beyond diagonal reconfigurable intelligent surfaces: A multi-sector mode enabling highly directional full-space wireless coverage," *IEEE J. Sel. Areas Commun.*, pp. 1–1, 2023.
- [33] —, "Synergizing beyond diagonal reconfigurable intelligent surface and rate-splitting multiple access," *IEEE Trans. Wireless Commun.*, pp. 1–1, 2024.
- [34] —, "A dynamic grouping strategy for beyond diagonal reconfigurable intelligent surfaces with hybrid transmitting and reflecting mode," *IEEE Trans. Veh. Technol.*, pp. 1–6, 2023.
- [35] Q. Li, M. El-Hajjar, I. Hemadeh, A. Shojaeifard, A. A. M. Mourad, B. Clerckx, and L. Hanzo, "Reconfigurable intelligent surfaces relying on non-diagonal phase shift matrices," *IEEE Trans. Veh. Technol.*, vol. 71, no. 6, pp. 6367–6383, 2022.
- [36] D. M. Pozar, *Microwave engineering*. John Wiley & sons, 2011.
- [37] S. Shen and R. D. Murch, "Impedance Matching for Compact Multiple Antenna Systems in Random RF Fields," *IEEE Trans. Antennas Propag.*, vol. 64, no. 2, pp. 820–825, 2016.
- [38] J. A. Bondy and U. S. R. Murty, *Graph theory with applications*. Macmillan London, 1976, vol. 290.
- [39] D. O’Leary and G. Stewart, "Computing the eigenvalues and eigenvectors of symmetric arrowhead matrices," *J. Comput. Phys.*, vol. 90, no. 2, pp. 497–505, 1990.
- [40] Z. H. Shaik, E. Björnson, and E. G. Larsson, "MMSE-optimal sequential processing for cell-free massive MIMO with radio stripes," *IEEE Trans. Commun.*, vol. 69, no. 11, pp. 7775–7789, 2021.
- [41] G. Strang, *Introduction to linear algebra*. Wellesley-Cambridge Press Wellesley, MA, 1993, vol. 3.